A New Prismatic Series Elastic Actuator with Compact Size and High Performance

Nicholas Paine and Luis Sentis

***Abstract*— This paper discusses design and control of a prismatic series elastic actuator with high mechanical power output in a small and lightweight form factor. We introduce a design that pushes the performance boundary of electric series elastic actuators by using high motor voltage coupled with an efficient drivetrain to enable large continuous actuator force while retaining speed. Compact size is achieved through the use of a novel piston-style ball screw support mechanism and a concentrically placed compliant element. We develop controllers for force and position tracking based on combinations of PID, model-based, and disturbance observer control structures. Finally, we demonstrate our actuator's performance with a series of experiments designed to operate the actuator at the limits of its mechanical and control capability.**

I. Introduction

Series Elastic Actuation (SEA) is a departure from the traditional approach of rigid actuation commonly used in factory room automation. Unlike rigid actuators, SEAs contain an elastic element in series with the mechanical energy source. The elastic element gives SEAs several unique properties compared to rigid actuators including low mechanical output impedance, tolerance to impact loads, increased peak power output, and passive mechanical energy storage [1], [2], [3].

A. SEA Design Background

Electric SEAs have been widely used in the fields of legged robotics and human orthotics [4]. Electric SEAs contain a motor to generate mechanical power, a speed reduction to amplify motor torque, a compliant element to sense force, and a transmission mechanism to route mechanical power to the output joint. There are many different possible implementations for these SEA elements, each with its advantages and disadvantages. [5], [6], [7] and [8] propose rotary designs based primarily on commercially available off-the-shelf parts, using a planetary gearbox for reduction, rotary or compression springs as the compliant element, and power transmission through a bevel gear [7] or chain/cable [5], [6]. For a more compact rotary actuator, other designs use backlash-free harmonic drives for the reduction and compact high-stiffness planar springs [9], [10]. [11] also uses a harmonic drive but chooses lower stiffness die springs to increase potential energy storage. [11], [12] use linear springs coupled to rotary shafts to achieve compact actuator packaging. [13] uses a novel worm-gear/rotary-spring/spur-gear design which allows the motor to be placed orthogonally to the joint axis at the cost of reduced efficiency and non-backdrivability due to the worm gear. [14] is similar in that it contains a spring within the speed reduction phase but uses two motors in parallel and has a relatively small reduction through a series of gears and a cable transmission. Both of the previous two designs place the spring within the reduction phase which reduces the torque requirement on the spring compared to designs with the spring at the output. With reduced torque compressing the spring, energy stored in the spring is reduced as well. [15], [16] and [17] propose prismatic designs which use highly efficient and backlash-free ball screws as the primary reduction mechanism followed by a cable drive to allow the actuator to remotely drive a revolute joint. [15] includes a belt drive between the motor and the ball screw which creates an additional speed reduction. Finally, [18] uses a ball screw and directly drives the joint with a pushrod style drive.

Variable stiffness actuators extend the SEA concept by adding an additional degree of freedom which is capable of mechanically adjusting the passive elastic stiffness [19], [20], [21], [22], [23]. Other SEA implementations have experimented with non-linear spring stretching to maximize energy storage [24].

B. SEA Control Background

Many different control architectures have been proposed for series elastic actuators. Control approaches can be roughly separated into different categories based on the types and combinations of control structures used. [25], [26] and [8] measure spring force and control motor force using some subset of PID control structures (P, PD, etc). If friction and backlash are too large then a pure high-gain PID approach can suffer from stability issues. To remedy this issue, [27] suggests using position feedback as the inner-most control structure for force control. This idea has been adopted and carried on by many others, treating force control as a position or velocity tracking problem [24], [9], [28], [29]. Such an approach relies on position feedback from the motor and the spring which naturally lends itself to position-encoder-based force feedback rather than load-cell-based force feedback. Another class of controllers use PID control but also consider the dynamics of the mechanical system to improve the frequency response of force control [1], [19]. [7] and [13] use PID, model-based, and disturbance observer structures together to achieve impressive torque tracking performance.

N. Paine is with the Department of Electrical and Computer Engineering, University of Texas, Austin, TX 78712 USA npaine@utexas.edu

L. Sentis is with the Department of Mechanical Engineering, University of Texas, Austin, TX 78712 USA lsentis@austin.utexas.edu

C. Actuator Performance

In this paper we define actuator performance by a combination of metrics which include measured power-to-weight ratio, force tracking accuracy and bandwidth, position tracking accuracy and bandwidth, force and position resolution, and efficiency. We summarize performance with the power-to-weight ratio and efficiency metrics since they are dependent on the performance of the other metrics and are easily represented with a single numerical value.

Detailed data on these performance metrics is not currently publicly available for most existing electric SEAs. [4] provides experimental data for peak power output for the actuator described in [30] and is able to achieve 64 W/kg. [31] provides the power exerted during a hop for the knee joint of [11] (close to 60 W), but because the actuators are integrated into a three degree-of-freedom leg, the actuator power-to-weight ratio is difficult to calculate.

D. Contributions and Paper Structure

This paper highlights research in development of the University of Texas Series Elastic Actuator (UT-SEA), a compact, light-weight, high-power actuator designed to enable energetic and high speed locomotion in electrically actuated legged systems (Figure 1). Our contributions include 1) a novel mechanical design that is more compact and lightweight than previous ball screw SEA designs, 2) an improvement on controller design and implementation methodology for force and position control of SEAs, 3) achievement of leading experimental results in the field of electric SEA performance (94 W/kg, 77% mechanical efficiency) which we believe may serve as a performance benchmark for other fixed-range-of-motion, passively cooled, high force electric actuators.

We first describe the design motivation behind the electrical power system and motor operation, followed by explanation of the actuator drivetrain and mechanical design. We then develop controllers for force and position based on a dynamic model of the actuator. Finally, we validate the entire system in hardware through a series of high performance experiments.

II. Design

Nature provides many examples of well designed actuators for legged applications. An average human adult male can produce 1500 watts of mechanical power during pedaling exercises, which corresponds to a whole-body power-to-weight ratio of 19.5 watts per kilogram [32]. To achieve similar performance in man-made legged machines, great care must be taken during the actuator design phase to maximize mechanical power output while keeping actuator size and weight small. Excess actuator weight reduces the whole-body power-to-weight ratio while large size limits a modular actuator's applicability in dense high-degree-of-freedom legged robot designs. Hydraulic actuation is one approach which achieves these goals but suffers from inefficient operation as discussed in [33].

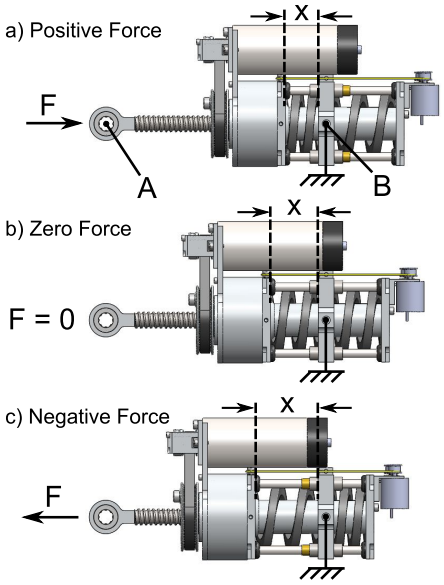

Fig. 1. UT-SEA operation for a fixed-displacement variable-force scenario. Actuator displacement is defined as the distance between points A and B. This distance remains constant while spring deflection (x) depends on actuator force.

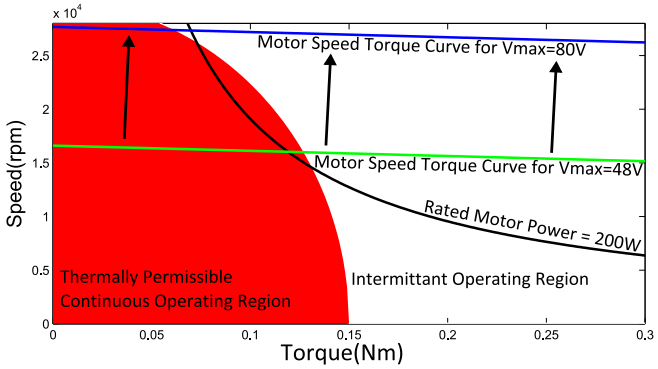

Fig. 2. Motor operating range for Maxon EC-powermax 30 as taken from the datasheet. A motor is capable of operating inside of the area below the speed-torque curve for a given applied voltage. Increasing voltage to 80V greatly increases the operating range of the motor, particularly in the continuous operating region.

We began the design process with a set of loose performance specifications (peak joint torques around 70Nm and maximum velocities around 15 rad/sec) obtained from simulations of legged locomotion in rough terrain and from discussions with other designers in the field. These values can be easily changed to design a similar actuator addressing alternate performance specifications. This flexibility is due to the high dimensionality of the UT-SEA design parameters.

A. Motor

High bus voltage is desirable to maximize achievable motor velocity and torque. Motor manufacturers typically provide a "rated voltage" for each motor which keeps transient motor current within reasonable values for common PWM frequencies (10 to 20kHz). However, larger voltages and thus greater mechanical power is possible as long as transient current is limited. For the UT-SEA we chose a

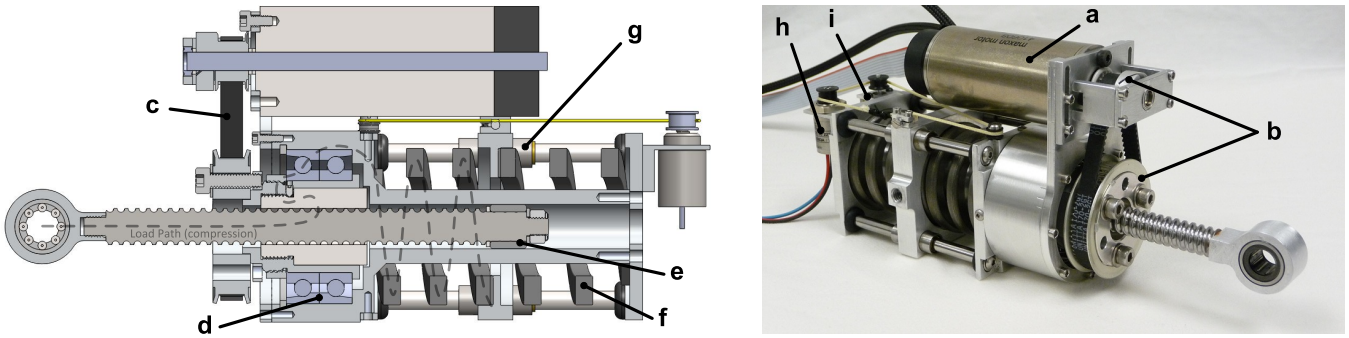

Fig. 3. Cross section of the UT-SEA showing drivetrain components including a) Maxon EC-4pole 30 200W BLDC motor, b) 3:1 pulley speed reduction, c) low backlash timing belt, d) angular contact bearings, e) piston-style ball screw support, f) high compliance springs, g) miniature ball bearing guides, h) absolute encoder, and i) incremental encoder. The compression load path is depicted as well.

Maxon EC-powermax 30 BLDC motor with a rated voltage of 48V. To increase mechanical power, we instead supply the motor with 80V (see Figure 2). We regulate transient motor current by using a 32kHz PWM servo drive (Elmo Ocarina 15/100) and additional high-current series inductors. Calculations provided by the drive manufacturer indicated that a series inductance of at least 0.082mH would keep transient current within reasonable values. The small added mass of the inductors is justified in that they allow the continuous force of the actuator to be increased by 66% without sacrificing output speed.

The high motor speed produced by high bus voltage enables the use of a large speed reduction which increases both intermittent and continuous torque capability compared to designs with lower voltages and lower speed reductions. These considerations indicated that a design using a speed reduction of approximately 175:1 would allow the actuator to meet the specified torque and speed requirements.

B. Drivetrain

To maximize mechanical power at the joint, energy must be transmitted from the motor to the joint with as few losses as possible. We chose a pulley/ball-screw speed reduction design similar to [15] for several reasons. A pulley/ball-screw reduction is efficient (typically above 90%), impact resistant, and backdrivable while the pulley ratio reduces the high motor speed to a speed more suitable for driving the ball screw.

Unlike [15] and other ball screw SEA designs, our design drives the ball nut instead of the ball screw ([34] uses a similar ball-nut-driven design but is a non-series-elastic cable-driven actuator). Driving the ball nut enables two key features which reduce the size and weight of the UT-SEA. First, ball screw support is incorporated directly into the actuator housing using an innovative piston-style guide (see Figure 3). This feature replaces the long, bulky rails used to support the output carriage in conventional prismatic SEA designs. Secondly, the compliant element is placed concentrically around the piston-style ball screw support which gives series elasticity without adding to the length of the actuator. These two features combine together to define the compact form factor of the UT-SEA.

The ball nut is supported by dual angular contact bearings which allow the ball nut to rotate within the housing while transmitting axial force from the ball nut to the housing. Custom preloaded die springs (manufactured by Diamond Wire Spring Co.) transmit force from the actuator housing to the chassis ground. The die springs are supported by four miniature ball bearing guide rails (Misumi) which are mounted to the housing using grommets that allow for slight misalignment during operation. The miniature ball bearing guides offer both lower friction and higher tolerance to torsional loads than bushing style guides. Force is sensed using a 20,000 count-per-revolution incremental encoder (Avago AEDA 3300) along with an absolute sensor (Novotechnik Vert-X 1302) to remove the need for startup calibration. A low stretch, low creep Vectran cable is attached to the chassis ground and is routed around the two spring deflection sensors using pulleys and an idler. Overall actuator position is measured combining readings from the motor encoder and the spring encoders. An absolute rotary sensor on the driven joint is used to initialize actuator position.

C. Spring Placement and Stiffness

There are two common arrangements of components found in SEA designs. The first arrangement, which we will refer to in this paper as Force Sensing Series Elastic Actuator (FSEA), places the compliant element between the gearbox output and the load. The second arrangement, which we will refer to as Reaction Force Sensing Series Elastic Actuator (RFSEA), places the spring between the motor housing and the chassis ground.

From a design standpoint there are several trade-offs between the two arrangements. RFSEA style actuators have the advantage of being more compact since the compliant element does not have to travel with the load but may be placed statically behind the actuator (or it can be remotely located as shown in [11], [12]). Prismatic RFSEAs also have greater range of motion for a given ball screw travel length compared to prismatic FSEAs as shown in Figure 4. The primary drawbacks of RFSEAs are less direct force sensing, reduced force tracking performance, and decreased protection from impact loads. An RFSEA style design was chosen to minimize the bounding volume of the UT-SEA. However, this design decision was heavily influenced by the

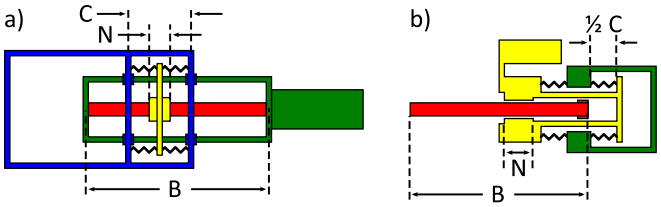

Fig. 4. Range of motion comparison between prismatic (a) FSEAs and (b) RFSEAs. For simplification, we assume that springs are fully compressible, spring plates have zero thickness, and the FSEA carriage travel is constrained to the length of the ball screw. The notations represent: B: ball screw length, C: carriage length, N: ball nut length. Range of motion is then $B - C$ for the FSEA and $B + C - N$ for the RFSEA.

TABLE I
UT-SEA SPECIFICATIONS

UT-SEA Design Specifications		
Weight	1168 g	2.575 lbs
Stroke	6 cm	2.36 in
Max Speed	32.5 cm/sec	12.79 in/sec
Continuous Force	848 N	190 lbs
Intermittent Force	2800 N	629 lbs
Spring Stiffness	278 N/mm	1587 lbs/in
Force Resolution	0.31 N	0.069 lbs
Operating Voltage	80V	

selection of the pushrod/ball-screw drivetrain. The drivetrain exhibited strong radial symmetry and possessed long, narrow ball screw support structure which allowed die springs to be integrated without excess bulk.

Spring stiffness for UT-SEA was chosen to maximize energy storage. For a given force, soft springs are able to store more energy than stiff springs. Peak force, desired deflection (maximum possible deflection to minimize stiffness), and the geometric constraints of the actuator were given as design specifications to Diamond Wire Spring Co. They then designed and manufactured a spring with a stiffness rate of 138 N/mm which effectively doubles to 277 N/mm for the actuator spring constant since two springs are used with precompression.

D. Design Summary

The end result of the design process is a pushrod RFSEA-style actuator that is compact enough to be placed at each joint of an articulated leg. Such small size enables a modular leg design similar to those seen in hydraulic robots [35], [36]. Articulated leg designs using linear actuators benefit from the nonlinear linkage kinematics created at the joint (refer to Figure 8). Torque generated by such a linkage has an angle dependent moment arm which can be used to provide high torque and high speed capability where they are needed (high torque when the leg is bent, high speed when the leg is extended). A summary of the design parameters for the actuator can be seen in Table I.

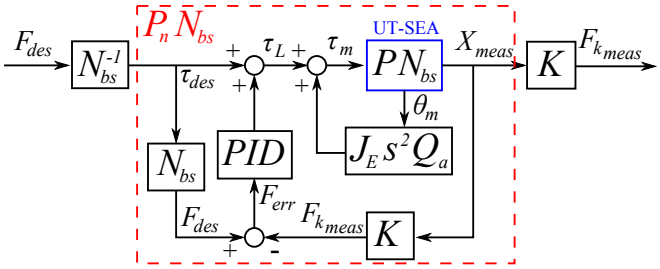

Fig. 5. PID force controller used for closed-loop system identification. The physical actuator is denoted by the "UT-SEA" block, which takes an input of motor torque and produces observable outputs motor position and spring position. N_{bs} is the actuator speed reduction and K is the spring constant. Q_a is a low-pass filter defined by (5).

III. CONTROL

Legged systems experience periods of high output impedance during stance phase and low output impedance during swing phase. A class of controllers that takes advantage of this discrepancy are Raibert-style controllers which use force control during stance phase to servo body attitude and position control during swing phase to regulate forward center-of-mass velocity [37]. This strategy suggests that actuators for legged systems should be capable of controlling both output force and position.

A. Force Control

The goal of force control is to make measured actuator output force track a desired force profile using motor torque (τ_m) as the plant input and measured spring deflection (X_{meas}) as the output. Not all of the torque generated by the motor produces force at the actuator output. During acceleration of motor angle (θ_m), a portion of the motor torque must accelerate the actuator's own effective internal inertia (J_E). The rest of the motor torque (τ_L) produces forces on the external actuator load.

$$\tau_m = J_E \ddot{\theta}_m + \tau_L \tag{1}$$

τ_L is the only component of motor torque that goes towards producing actuator output force, so a compensator is used to maintain τ_L at some desired torque, τ_{des} (see Figure 5). The compensator consists of a feedforward term and a feedback term. The feedback attempts to keep the difference between desired force (F_{des}) and measured spring force ($F_{k_{meas}}$) small. F_{des} is calculated using τ_{des} multiplied by the force amplification due to the speed reduction of the gearbox (N_{bs}). For the UT-SEA, the speed reduction results from a pulley reduction (N_p) and a ball screw, which is parameterized by drivetrain efficiency (η) and ball screw lead (l). The speed reduction defines the relation between actuator force (F) and motor torque (τ).

$$N_{bs} = \frac{F}{\tau} = \frac{2\pi N_p \eta}{l} \tag{2}$$

Measured spring force is calculated using spring deflection and Hooke's Law: $F_{k_{meas}} = kx$.

Due to stability limitations, PID gains can only be increased up to certain values. To improve force tracking

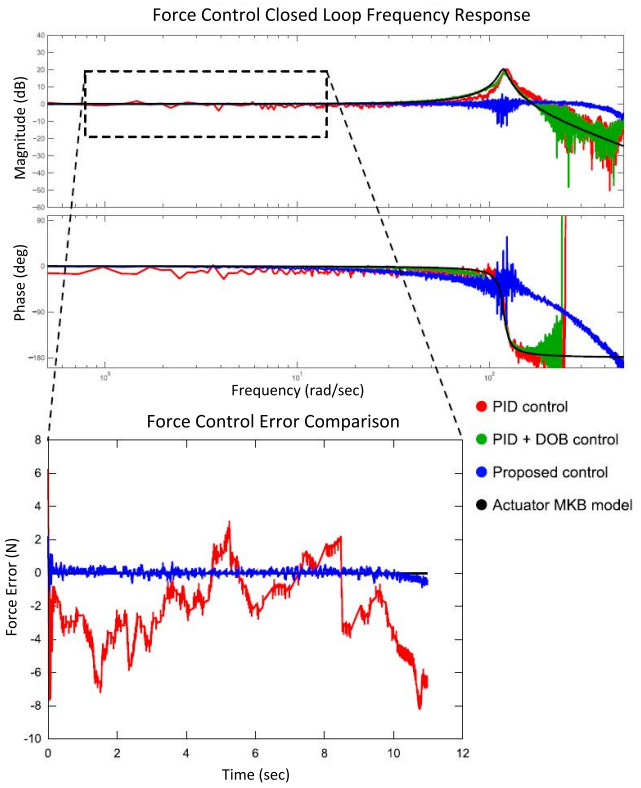

Fig. 6. Frequency response of incremental improvements to the force controller beginning with simple PID (Figure 5) and ending with the proposed controller (Figure 7). The black line is the mass-spring-damper model obtained using experimental system identification. Both PID + DOB and the proposed control greatly improve force tracking at low frequencies compared to pure PID control as shown in the detail view. The proposed controller improves on the PID + DOB control by removing large amplitude resonant oscillations, creating a response that stays close to 0 dB. All responses represent $F_{k_{meas}}/F_{des}$. Note that the detailed view is plotted on linear axes in the time domain but represents the same data shown in the main figure.

performance further and to remove steady state error another control approach is required. As demonstrated by [38], a disturbance observer (DOB) may be used to 1) measure and remove disturbances and 2) reduce the effect of plant modeling error. In particular, to use a DOB a nominal plant model is required. For this application, the DOB plant is the closed-loop transfer function (P_nN_{bs}) created by the PID controller shown in Figure 5 acting on the physical actuator (PN_{bs}). To obtain an accurate representation of the plant, we implement the controller shown in Figure 5 in hardware and perform system identification of P_nN_{bs} using an exponential chirp signal for F_{des} and fixing the actuator output. Plotting the frequency response of the magnitude and phase of $F_{k_{meas}}/F_{des}$ (red line in Figure 6) clearly identifies a second-order system, which we model as a simple mass-spring-damper. With k measured before actuator assembly, the only unknowns are m_k and b_{eff}. Fitting the mass-spring-damper model to the experimental data results in m_k = 19.75 kg and b_{eff} = 500 Ns/m and a damped resonant frequency of 18hz. This model is shown as the black line in Figure 6. Dividing the model's transfer function (which represents $F_{k_{meas}}/F_{des}$) by k yields the X_{meas}/F_{des} transfer function:

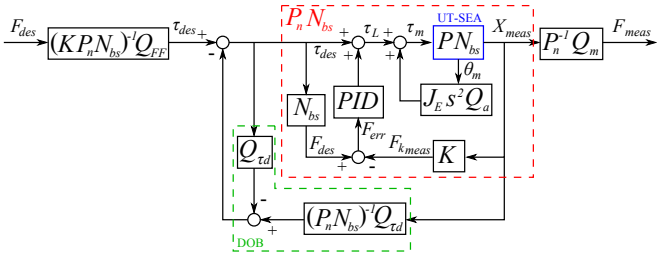

Fig. 7. Block diagram of the proposed force control structure. The physical actuator is denoted by the "UT-SEA" block. The Q functions are low-pass filters defined by (5).

$$P_n = \frac{X_{meas}(s)}{F_{des}(s)} = \frac{1}{s^2 m_k + s b_{eff} + k} \tag{3}$$

Combining (2) and (3) fully characterizes the dynamics of the nominal DOB plant from τ_{des} to X_{meas}:

$$P_nN_{bs} = \frac{X_{meas}(s)}{F_{des}(s)} \frac{F_{des}(s)}{\tau_{des}(s)} = \frac{X_{meas}(s)}{\tau_{des}(s)} \tag{4}$$

With the nominal DOB plant defined, the DOB is incorporated into the force controller as shown in Figure 7. Measuring the frequency response of the controller with the DOB added shows improved tracking performance compared to PID control (green line in Figure 6). In fact, low frequency force tracking error is reduced 93% by adding the DOB to the PID controller (Figure 6 detail). The DOB forces the closed-loop response to fit closely to the mass-spring-damper model. The DOB includes a filter ($Q_{\tau d}$) which is required to make the inverse plant model realizable and to attenuate high frequency disturbances. $Q_{\tau d}$, with the rest of the Q functions depicted in Figures 5, 7, and 9, is implemented as a low-pass Butterworth filter and has the following transfer function:

$$Q(s) = \frac{1}{(s/\omega_c)^2 + 1.4142(s/\omega_c) + 1} \tag{5}$$

The cutoff frequency of each filter (ω_c) was determined empirically and in general should be set higher than the desired closed-loop control bandwidth of the application.

Ideally, the magnitude of the closed-loop transfer function of the force controller should be close to one (0 dB) over some desired bandwidth. As can be seen in Figure 6, the PID + DOB controller amplifies spring force by 20 dB (a factor of 10) for excitation signals close to the resonant frequency. To remove this resonance, a feedforward filter is introduced which is created using the inverse nominal plant dynamics multiplied by the spring constant ($(KP_nN_{bs})^{-1}$ in Figure 7). A low-pass filter (Q_{FF}) is again used to make the inverse transfer function realizable. Finally, although output force is not used in the force feedback loop, a filter is used to generate actuator force from spring deflection measurement ($P_n^{-1}Q_m$ in Figure 7) which is used for observation purposes.

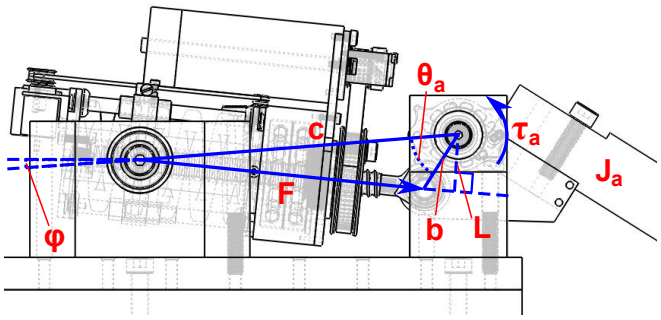

Fig. 8. UT-SEA mounted on a test bench with the prismatic linkage geometry shown. The notations represent: L: linkage moment arm, c: distance between the actuator pivot and the arm pivot, b: distance between the arm pivot and the push rod pivot, F: actuator force, τ_a: torque exerted on the output arm, θ_a: output arm angle, J_a: inertia of the output arm, ϕ: offset angle. Values used during testing of the actuator are: b=0.025 [m], c=0.125 [m].

B. Position Control

Fast, stable position control is crucial for high speed legged locomotion, especially during swing phase. By using the aforementioned force controller as the innermost component of the position controller, we are able to treat the actuator as a nearly ideal force source. This force source generates a torque through a mechanical linkage with a moment arm (L) as depicted in Figure 8. Actuator force (F) generates arm torque (τ_a) depending on arm angle (θ_a) according to the following equation.

$$\tau_a = FL(\theta_a) = F\frac{cb\sin\theta_a}{\sqrt{b^2+c^2-2bc\cos\theta_a}} \tag{6}$$

The dynamics relating τ_a to θ_a with arm inertia (J_a) and joint friction (B_a) are:

$$\tau_a = J_a\ddot{\theta}_a + B_a\dot{\theta}_a + \tau_g(\theta_a) \tag{7}$$

where τ_g is the torque due to gravity and is parameterized by the mass of the output link (m_a), the distance from the point of rotation to the center of mass (l_m) and an angle (ϕ) to correct for c in Figure 8 not being orthogonal to the gravity vector.

$$\tau_g(\theta_a) = -m_a g l_m \cos(\theta_a + \phi) \tag{8}$$

Combining (6) (7) and (8) the full dynamics from F to θ_a are then represented by the following nonlinear differential equation.

$$F = \frac{\sqrt{b^2+c^2-2bc\cos\theta_a}}{cb\sin\theta_a}\Big[J_a\ddot{\theta}_a + B_a\dot{\theta}_a - m_a g l_m\cos(\theta_a+\phi)\Big] \tag{9}$$

Our position control approach first considers the problem of controlling θ_a given τ_a. The relation between τ_a and θ_a is given as:

$$\frac{\theta_a}{\tau_a} = \frac{1}{s^2 J_a + sB_a} \tag{10}$$

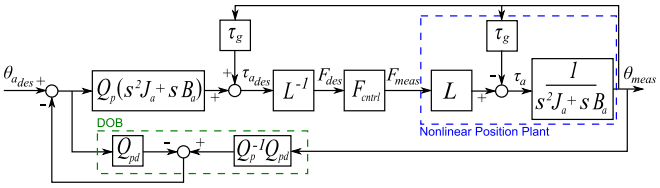

Fig. 9. Block diagram of the control structure used for position control. The notations represent: τ_g: gravity compensation torque, L: nonlinear linkage kinematics, F_{cntrl}: the force control block shown in Figure 7. The Q functions are low-pass filters defined by (5).

Inverting (10) provides a desired arm torque ($\tau_{a_{des}}$) given a desired arm angle ($\theta_{a_{des}}$) and is used as the initial block in the position controller (Figure 9). Because (10) does not consider gravity, the desired arm torque signal must be summed with a gravity compensation torque (8) to produce the expected motion. The resulting torque value is then converted into desired actuator force by multiplying by the inverse of the nonlinear kinematics (L^{-1} from (6)). This desired force is then passed to the force controller.

Without some form of feedback the position controller would not be able to track a desired position due to modeling error and external disturbances. A DOB is placed in an outer loop around the model-based position controller to resolve these issues. The DOB treats modeling error and exogenous input as a disturbance and counteracts this disturbance with input to the model-based position controller. Q_p in Figure 9 is a feed forward low-pass filter to smooth position response, thus reducing required torques. Q_{pd} is a low-pass filter that attenuates high frequency disturbance signals of the DOB.

IV. Performance Experiments and Energetics

Our goal was to design hardware and controllers that would maximize performance, but how do we know if we have been successful? One way of measuring the success of the control design is to attempt to reach the mechanical limits of actuator components in a safe and controlled manner. To this end we performed an experiment to push actuator speed

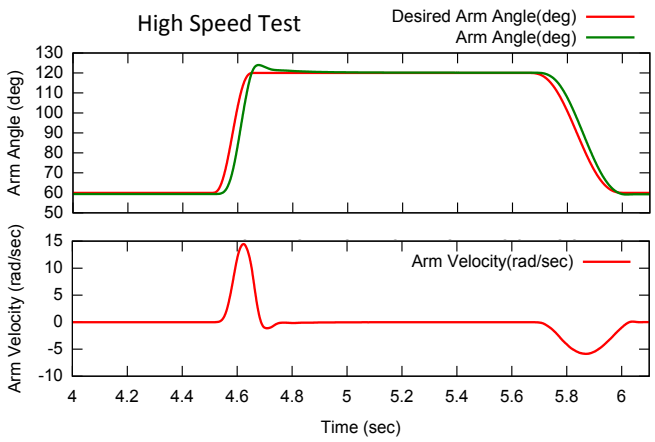

Fig. 10. High speed position tracking test. The actuator output follows a reference signal that changes 60 degrees in less than 0.2 seconds. The actuator is able to track the reference signal closely and reaches the maximum mechanical speed of the ball screw of 15 rad/sec.

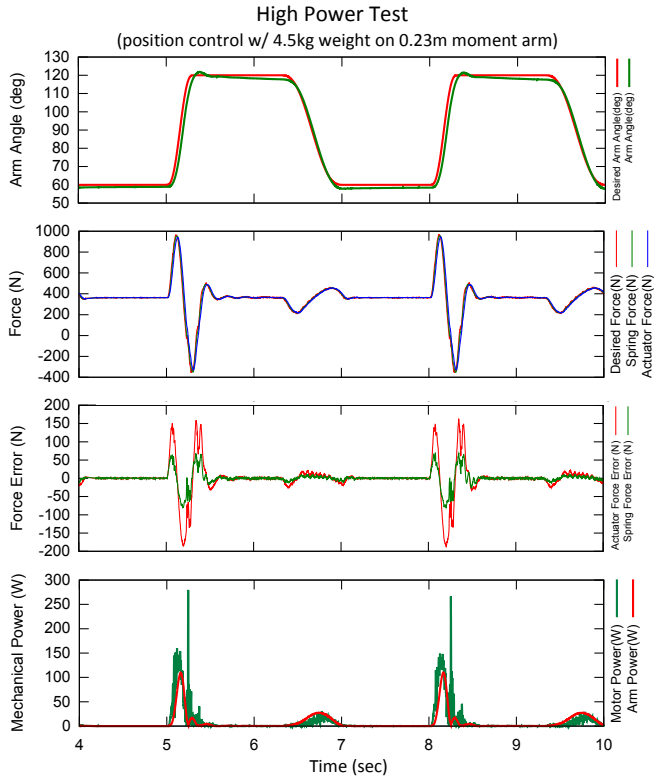

Fig. 11. Data from the high power test. Accuracy of both position and force tracking can be seen in the top two graphs. The third graph shows force error of both spring force and output force. The bottom graph shows power measured at the motor (desired torque time motor velocity) and at the output (measured torque times measured velocity).

to the limits of mechanical and control capabilities. A 5th order spline was used to generate a smooth position reference signal for high speed transitions between a large angle displacement (60 degrees). Figure 10 shows the experimental results. The arm is able to track the reference position closely and achieves a velocity of 15 rad/sec which is the mechanical limit of the ball screw. In this test, the motor reached a speed of 22,600 rpm which is 3,000 rpm below the maximum possible motor speed. Acceleration from rest, to maximum speed, and back to rest occurs within less than 0.2 seconds.

Arguably one of the most important metrics for performance is power output. To maximize achievable power we designed an experiment which would require high speed and high torque simultaneously. Figure 11 shows the experimental results. The actuator generates peak mechanical output power of approximately 110 watts, which corresponds to a power-to-weight ratio of 94 watts per kilogram. Comparing with [4] this represents a 47% improvement over previous attempts. While these are strong results, we believe that the actuator is capable of much higher output. We plan to test this hypothesis in future design iterations.

We present one final experiment aimed at measuring actuator efficiency. We designed an experiment to measure the efficiency of power transfer from the output of the motor to the output of the actuator. Figure 12 shows the experimental results. Efficiency in the forward direction from the motor to the output (η_f) was measured to be 77% while efficiency

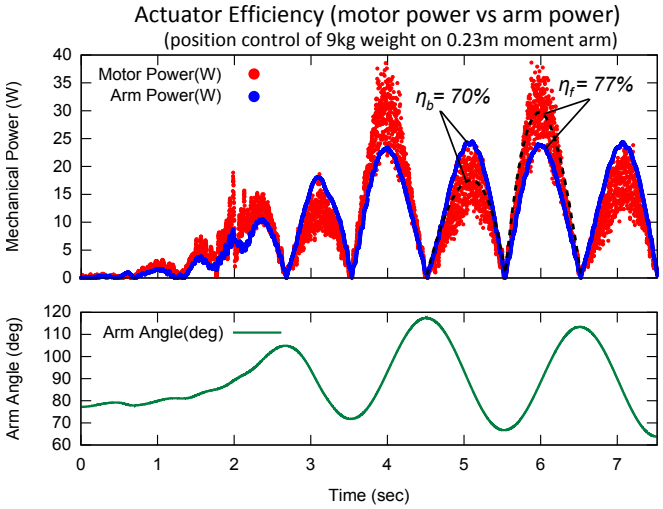

Fig. 12. Test to measure actuator mechanical efficiency. The arm is tracking a sinusoidal position reference with weight added. Motor power is calculated from desired motor torque times measured motor velocity while arm power is calculated from measured arm torque times measured arm velocity. η_f and η_b represent forward and backward efficiency, respectively. On upward swings, motor power is greater than arm power because the actuator must work against gravity. On downward swings, arm power is greater than motor power due to gravity backdriving the actuator.

in the reverse direction (η_b) was 70%. This experiment does not consider the efficiency of converting electrical power into mechanical power of the motor. However, efficiency of the motor drive's H-bridge and the efficiency of the motor can be very high, mostly depending on motor torque and speed. We plan to measure this efficiency in future work.

V. Conclusions

This paper introduced the UT-SEA, a compact, lightweight, high-power actuator designed to empower the next generation of electrically actuated legged machines. Unlike other prismatic SEAs, the UT-SEA features a tightly integrated pushrod design which allows the actuator to be housed within a robotic leg and use a nonlinear mechanical linkage to drive a rotary joint. High motor voltage and current filtering enable the use of a large speed reduction which significantly increases both continuous and peak torque capabilities. Placement of the elastic element between the actuator housing and chassis ground creates a design with increased range of motion and compactness.

We presented a SEA controller design based on model-based, PID, and disturbance observer structures and validated the controller in hardware. The proposed force controller was able to track forces with 93% less error than conventional PID-based control for low frequency signals and removed harmful spring resonance associated with RFSEA designs. We also presented a model-based position controller which includes the proposed force controller as the innermost loop. We performed high speed tracking experiments with this controller and achieved speeds of 15 rad/sec which is the mechanical limit of the hardware. Additional tests showed peak actuator power of 110 watts and mechanical efficiency of 77%.

REFERENCES

[1] G. Pratt and M. Williamson, "Series elastic actuators," in *Intelligent Robots and Systems 95. 'Human Robot Interaction and Cooperative Robots', Proceedings. 1995 IEEE/RSJ International Conference on*, vol. 1, Aug 1995, pp. 399 –406 vol.1.

[2] S. Arumugom, S. Muthuraman, and V. Ponselvan, "Modeling and application of series elastic actuators for force control multi legged robots," *Journal of Computing*, vol. 1, 2009.

[3] D. Paluska and H. Herr, "Series elasticity and actuator power output," in *Robotics and Automation, 2006. ICRA 2006. Proceedings 2006 IEEE International Conference on*, May 2006, pp. 1830 –1833.

[4] J. Pestana, R. Bobin, J. C. Arevalo, and E. Garcia Armada, "Characterization of emerging actuators for empowering legged robots," in *CLAWAR*, 2010.

[5] S. Curran and D. Orin, "Evolution of a jump in an articulated leg with series-elastic actuation," in *Robotics and Automation, 2008. ICRA 2008. IEEE International Conference on*, May 2008, pp. 352 –358.

[6] M. Hutter, C. Remy, and R. Siegwart, "Design of an articulated robotic leg with nonlinear series elastic actuation," in *Proc. of The 12th International Conference on Climbing and Walking Robots and the Support Technologies for Mobile Machines (CLAWAR)*, September 2009, pp. 645–652.

[7] K. Kong, J. Bae, and M. Tomizuka, "Control of rotary series elastic actuator for ideal force-mode actuation in human-robot interaction applications," *Mechatronics, IEEE/ASME Transactions on*, vol. 14, no. 1, pp. 105 –118, Feb. 2009.

[8] D. Ragonesi, S. Agrawal, W. Sample, and T. Rahman, "Series elastic actuator control of a powered exoskeleton," in *Engineering in Medicine and Biology Society,EMBC, 2011 Annual International Conference of the IEEE*, Sept. 2011, pp. 3515 –3518.

[9] C. Lagoda, A. Schouten, A. Stienen, E. Hekman, and H. van der Kooij, "Design of an electric series elastic actuated joint for robotic gait rehabilitation training," in *Biomedical Robotics and Biomechatronics (BioRob), 2010 3rd IEEE RAS and EMBS International Conference on*, Sept. 2010, pp. 21 –26.

[10] M. Diftler, J. Mehling, M. Abdallah, N. Radford, L. Bridgwater, A. Sanders, R. Askew, D. Linn, J. Yamokoski, F. Permenter, B. Hargrave, R. Piatt, R. Savely, and R. Ambrose, "Robonaut 2 - the first humanoid robot in space," in *Robotics and Automation (ICRA), 2011 IEEE International Conference on*, May 2011, pp. 2178 –2183.

[11] M. Hutter, C. Remy, M. Hoepflinger, and R. Siegwart, "ScarlETH: Design and control of a planar running robot," in *Proc. of the IEEE/RSJ International Conference on Intelligent Robots and Systems (IROS)*, 2011.

[12] E. Torres-Jara and J. Banks, "A simple and scalable force actuator," in *International Simposium of Robotics*, March 2004.

[13] K. Kong, J. Bae, and M. Tomizuka, "A compact rotary series elastic actuator for human assistive systems," *Mechatronics, IEEE/ASME Transactions on*, vol. 17, no. 2, pp. 288 –297, April 2012.

[14] M. D. Taylor, "A compact series elastic actuator for bipedal robots with human-like dynamic performance," Masters Thesis, Carnegie Mellon University, 2011.

[15] A. Edsinger-Gonzales and J. Weber, "Domo: a force sensing humanoid robot for manipulation research," in *Humanoid Robots, 2004 4th IEEE/RAS International Conference on*, vol. 1, Nov. 2004, pp. 273 – 291 Vol. 1.

[16] P. Gregorio, M. Ahmadi, and M. Buehler, "Design, control, and energetics of an electrically actuated legged robot," *Systems, Man, and Cybernetics, Part B: Cybernetics, IEEE Transactions on*, vol. 27, no. 4, pp. 626 –634, Aug 1997.

[17] J. Pratt and G. Pratt, "Intuitive control of a planar bipedal walking robot," in *Robotics and Automation, 1998. Proceedings. 1998 IEEE International Conference on*, vol. 3, May 1998, pp. 2014 –2021 vol.3.

[18] D. Robinson, J. Pratt, D. Paluska, and G. Pratt, "Series elastic actuator development for a biomimetic walking robot," in *Advanced Intelligent Mechatronics, 1999. Proceedings. 1999 IEEE/ASME International Conference on*, 1999, pp. 561 –568.

[19] J. Hurst, J. Chestnutt, and A. Rizzi, "The actuator with mechanically adjustable series compliance," *Robotics, IEEE Transactions on*, vol. 26, no. 4, pp. 597 –606, Aug. 2010.

[20] T.-H. Huang, J.-Y. Kuan, and H.-P. Huang, "Design of a new variable stiffness actuator and application for assistive exercise control," in *Intelligent Robots and Systems (IROS), 2011 IEEE/RSJ International Conference on*, Sept. 2011, pp. 372 –377.

[21] N. G. Tsagarakis, I. Sardellitti, and D. G. Caldwell, "A new variable stiffness actuator (CompAct-VSA): Design and modelling," in *Intelligent Robots and Systems (IROS), 2011 IEEE/RSJ International Conference on*, Sept. 2011, pp. 378 –383.

[22] M. Grebenstein, A. Albu-Schaffer, T. Bahls, M. Chalon, O. Eiberger, W. Friedl, R. Gruber, S. Haddadin, U. Hagn, R. Haslinger, H. Hoppner, S. Jorg, M. Nickl, A. Nothhelfer, F. Petit, J. Reill, N. Seitz, T. Wimbock, S. Wolf, T. Wusthoff, and G. Hirzinger, "The DLR hand arm system," in *Robotics and Automation (ICRA), 2011 IEEE International Conference on*, May 2011, pp. 3175 –3182.

[23] A. Jafari, N. G. Tsagarakis, and D. G. Caldwell, "A novel intrinsically energy efficient actuator with adjustable stiffness (AwAS)," *Mechatronics, IEEE/ASME Transactions on*, vol. PP, no. 99, pp. 1 –11, 2011.

[24] I. Thorson and D. Caldwell, "A nonlinear series elastic actuator for highly dynamic motions," in *Intelligent Robots and Systems (IROS), 2011 IEEE/RSJ International Conference on*, Sept. 2011, pp. 390 – 394.

[25] J. W. Sensinger and R. F. Weir, "Unconstrained impedance control using a compact series elastic actuator," in *Mechatronic and Embedded Systems and Applications, Proceedings of the 2nd IEEE/ASME International Conference on*, Aug. 2006, pp. 1 –6.

[26] E. Garcia, J. Arevalo, F. Sanchez, J. Sarria, and P. Gonzalez-de Santos, "Design and development of a biomimetic leg using hybrid actuators," in *Intelligent Robots and Systems (IROS), 2011 IEEE/RSJ International Conference on*, Sept. 2011, pp. 1507 –1512.

[27] G. Pratt, P. Willisson, C. Bolton, and A. Hofman, "Late motor processing in low-impedance robots: impedance control of series-elastic actuators," in *American Control Conference, 2004. Proceedings of the 2004*, vol. 4, July 2004, pp. 3245 –3251 vol.4.

[28] H. Vallery, R. Ekkelenkamp, H. van der Kooij, and M. Buss, "Passive and accurate torque control of series elastic actuators," in *Intelligent Robots and Systems, 2007. IROS 2007. IEEE/RSJ International Conference on*, 29 2007-nov. 2 2007, pp. 3534 –3538.

[29] G. Wyeth, "Control issues for velocity sourced series elastic actuators," in *Australian Conference on Robotics and Automation*, December 2006.

[30] J. E. Pratt and B. T. Krupp, "Series elastic actuators for legged robots," *Proc. SPIE 5422, Unmanned Ground Vehicle Technology VI*, pp. 135–144, 2004.

[31] M. Hutter, C. Remy, M. Hoepflinger, and R. Siegwart, "High compliant series elastic actuation for the robotic leg ScarlETH," in *Proc. of the International Conference on Climbing and Walking Robots (CLAWAR)*, 2011.

[32] A. Beelen and A. J. Sargeant, "Effect of fatigue on maximal power output at different contraction velocities in humans," *Journal of Applied Physiology*, vol. 71, no. 6, pp. 2332–2337, 1991. [Online]. Available: http://jap.physiology.org/content/71/6/2332.abstract

[33] A. Zoss, H. Kazerooni, and A. Chu, "Biomechanical design of the berkeley lower extremity exoskeleton (BLEEX)," *Mechatronics, IEEE/ASME Transactions on*, vol. 11, no. 2, pp. 128 –138, April 2006.

[34] P. Garrec, "Design of an anthropomorphic upper limb exoskeleton actuated by ball-screws and cables," in *Scientific Bulletin, Series D*, vol. 72, no. 2, 2010.

[35] M. Raibert, K. Blankespoor, G. Nelson, R. Playter, and T. B. Team, *BigDog, the Rough-Terrain Quadruped Robot*, 2008, pp. 10 822–10 825. [Online]. Available: http://www.df.unibo.it/divulgazione/attualita/bigdog.pdf

[36] C. Semini, N. Tsagarakis, E. Guglielmino, and D. Caldwell, "Design and experimental evaluation of the hydraulically actuated prototype leg of the HyQ robot," in *Intelligent Robots and Systems (IROS), 2010 IEEE/RSJ International Conference on*, Oct. 2010, pp. 3640 –3645.

[37] M. H. Raibert, *Legged Robots That Balance*. Cambridge, Mass: MIT Press, 1986.

[38] H. S. Lee and M. Tomizuka, "Robust motion controller design for high-accuracy positioning systems," *Industrial Electronics, IEEE Transactions on*, vol. 43, no. 1, pp. 48 –55, Feb 1996.